HHS Public Access

Author manuscript

Phys Med Biol. Author manuscript; available in PMC 2016 January 06.

Published in final edited form as:

Phys Med Biol. 2013 July 7; 58(13): 4513–4534. doi:10.1088/0031-9155/58/13/4513.

Phase-transition thresholds and vaporization phenomena for ultrasound phase-change nanoemulsions assessed via high speed optical microscopy

Paul S. Sheeran[1], **Terry O. Matsunaga**[2], and **Paul A. Dayton**[1,3]

[1]Joint Department of Biomedical Engineering, The University of North Carolina and North Carolina State University, Chapel Hill, NC 27599, USA

[2]Department of Medical Imaging, University of Arizona, Tucson, AZ 85724, USA

Abstract

Ultrasonically activated phase-change contrast agents (PCCAs) based on perfluorocarbon droplets have been proposed for a variety of therapeutic and diagnostic clinical applications. When generated at the nanoscale, droplets may be small enough to exit the vascular space and then be induced to vaporize with high spatial and temporal specificity by externally-applied ultrasound. The use of acoustical techniques for optimizing ultrasound parameters for given applications can be a significant challenge for nanoscale PCCAs due to the contributions of larger outlier droplets. Similarly, optical techniques can be a challenge due to the sub-micron size of nanodroplet agents and resolution limits of optical microscopy. In this study, an optical method for determining activation thresholds of nanoscale emulsions based on the *in vitro* distribution of bubbles resulting from vaporization of PCCAs after single, short (<10 cycles) ultrasound pulses is evaluated. Through ultra-high-speed microscopy it is shown that the bubbles produced early in the pulse from vaporized droplets are strongly affected by subsequent cycles of the vaporization pulse, and these effects increase with pulse length. Results show that decafluorobutane nanoemulsions with peak diameters on the order of 200 nm can be optimally vaporized with short pulses using pressures amenable to clinical diagnostic ultrasound machines.

Keywords

perfluorocarbon droplet; acoustic vaporization; contrast agent; phase-change; ultrasound; high-speed microscopy

1. Introduction

Though research in the field of microbubble-based contrast agents for ultrasound has been ongoing for more than 40 years (Gramiak and Shah 1968, Stride and Coussios 2010, Martin and Dayton 2013), many promising alternative contrast agents have emerged within the last decade. Among these, the phase-change contrast agent (PCCA) has been proposed for a

[3]Author to whom any correspondence should be addressed, padayton@bme.unc.edu, Address: 304 Taylor Hall, CB 7575, Chapel Hill, NC 27599, Phone: (919) 843-9521, Fax: (919) 843-9520.

wide range of applications as a result of its unique functionality (Rapoport 2012, Sheeran and Dayton 2012). When generated at microscale and nanoscale sizes, perfluorocarbon-based PCCAs have shown preclinical promise as highly-dynamic agents for applications such as selective vascular occlusion (Kripfgans *et al.* 2000, Kripfgans *et al.* 2002, Kripfgans *et al.* 2005, Zhang *et al.* 2010), cavitation nucleation enhancement and acoustic ablation (Miller *et al.* 2000, Zhang and Porter 2010, Zhang *et al.* 2011, Phillips *et al.* 2013), generation of *in vivo* contrast (Kripfgans *et al.* 2000, Haworth *et al.* 2008, Reznik *et al.* 2011, Sheeran *et al.* 2011b, Wang *et al.* 2012b, Wang *et al.* 2012a, Couture *et al.* 2012, Sheeran *et al.* 2013), therapeutic delivery (Rapoport *et al.* 2009b, Fabiilli *et al.* 2010b, Fabiilli *et al.* 2010a, Rapoport *et al.* 2011, Couture *et al.* 2012, Javadi *et al.* 2012, Lattin *et al.* 2012), and integration with other imaging modalities (Rapoport *et al.* 2011, Strohm *et al.* 2011, Wilson *et al.* 2012, Strohm *et al.* 2012). The utility of PCCAs stems primarily from their ability to be used in both the liquid and gas states, and the use of a non-invasive modality (ultrasound) to trigger this transition both temporally and spatially. Once the transition to the gaseous phase begins, a dramatic increase in the agent volume occurs, resulting in a bubble as much as an order of magnitude larger than the original droplet (Evans *et al.* 2006, Sheeran *et al.* 2011b, Reznik *et al.* 2011, Reznik *et al.* 2012). This externally-triggered transition gives the researcher high control over aspects such as size, stability, and level of agent interaction with the incident ultrasound beam.

Numerous studies have proposed and investigated nanoscale PCCAs that, once vaporized, form microbubbles ideal for ultrasound imaging contrast and cavitation within the ultrasound beam (i.e. having resonance frequencies near the insonation frequency) (Rapoport *et al.* 2009a, Reznik *et al.* 2011, Sheeran *et al.* 2011b, Sheeran *et al.* 2013). Such an agent would have utility for applications where imaging, drug delivery, and ablation are facilitated by passive diffusion of agents via the enhanced permeability and retention effect of solid tumors (Campbell 2006), as well as the potential to be used for general diagnostic/molecular imaging of other vascular targets. Determining appropriate ultrasonic conditions to initiate vaporization is vital for understanding both the physics behind droplet interactions with the ultrasound beam and for developing practical *in vivo* sequences for each application. However, measuring the phase-transition conditions for these nanoemulsions is complicated by a variety of factors. For a bulk compound, the phase-transition temperature and pressure can be predicted simply, but for micro- and nanoemulsions of the same compound, scaling effects significantly alter these properties. The internal pressure of the droplet is increased beyond ambient pressure as a result of the Laplace pressure – and reaches several additional atmospheres of pressure for perfluorocarbon droplets with diameters in the 100s of nanometers (Evans *et al.* 2006, Rapoport *et al.* 2009b, Sheeran *et al.* 2011b, Sheeran *et al.* 2011a). This greatly increases the ‘effective’ boiling point (boiling point elevation) as well as the ultrasound intensity necessary for vaporization. In addition, myriad other factors of droplet design, ambient conditions, and ultrasound parameters have been shown to influence activation of phase-change perfluorocarbon droplets (Kripfgans *et al.* 2000, Kripfgans *et al.* 2002, Giesecke and Hynynen 2003, Lo *et al.* 2007, Fabiilli *et al.* 2009, Schad and Hynynen 2010, Sheeran and Dayton 2012, Shpak *et al.* 2013). As such, a model to predict the phase-transition point of an individual droplet that incorporates these influences is yet to be developed.

Researchers have instead approached determining phase-transition conditions for their emulsions experimentally. Historically, measuring activation has taken two forms: direct and phenomenological. In order to discern the underlying physics (precise relations between droplet design and the phase-transition point), the minimum ultrasound conditions required to vaporize a droplet are typically of interest. As such, direct measurements often involve high-magnification microscopy and high-speed imaging such that researchers can isolate individual droplets optically and observe the phase-transition as it occurs while manipulating the activation parameters (Kripfgans *et al.* 2004, Strohm *et al.* 2011, Sheeran *et al.* 2011b, Sheeran *et al.* 2012). By gathering a large number of observations, general trends and conclusions can be drawn regarding the relationship of activation parameters with the variety of design factors. However, if the desire is to ultimately use the agents *in vivo*, measurements must incorporate spatial aspects of vaporization such as degree of activation in a region where many droplets are present (as the goal is rarely to activate only a single droplet). Therefore, those more interested in measuring how well the emulsions can deliver a desired effect typically approach measures of activation through phenomenological means, such as echo/image/fluorescence intensity (Kripfgans *et al.* 2000, Lo *et al.* 2007, Fabiilli *et al.* 2009, Couture *et al.* 2011, Couture *et al.* 2012), reduction in blood flow (Kripfgans *et al.* 2005, Zhang *et al.* 2010), degree of stable or inertial cavitation (Giesecke and Hynynen 2003, Fabiilli *et al.* 2009, Schad and Hynynen 2010), size of lesion or bubble cloud formed (Zhang *et al.* 2011, Lo *et al.* 2006, Phillips *et al.* 2013), tumor volume reduction and cell death (Miller and Song 2002, Rapoport *et al.* 2009b, Martin *et al.* 2012), and degree of thermal or drug/gene delivery (Miller and Song 2002, Zhang and Porter 2010). By altering the activation parameters and observing the change in a desired effect, practical activation conditions can be determined.

Each of these approaches can be extremely limiting with regard to determining phase-transition thresholds for nanoemulsions, in particular. Direct optical observations do not allow measure of the initial size of individual particles below ~800 nm with reasonable accuracy due to brightfield resolution limits (though they are visible at sizes > 500 nm), so trends for larger microscale particles must be used to predict parameters at the nanoscale (Sheeran *et al.* 2011b). The accuracy of these trends through the entire nanoscale must be called into question. In addition, the interaction between the acoustic beam and the experimental setup (often a microcellulose tube) can lead to a heterogeneous pressure distribution within the tube and introduce a high level of spatial variation in results (Kripfgans *et al.* 2004, Qin *et al.* 2008). Lastly, methods of producing PCCAs often result in polydisperse emulsions, as is commonly the case for nanoscale agents (Kawabata *et al.* 2005, Rapoport *et al.* 2009b, Zhang and Porter 2010, Reznik et al 2011, 2013 Sheeran *et al.* 2011a, Sheeran *et al.* 2012, Sheeran *et al.* 2013). Because bubble nucleation is a stochastic process (Brennen 1995), and because an inverse relationship between particle size and vaporization pressure exists, larger droplets will phase-shift with greater efficiency at a given ultrasound pressure. Even a small presence of large outliers can highly skew phenomenological measures such as echogenicity/echo amplitude as the contribution by larger particles overshadows the more subtle contribution of the nanoscale particles. Though the researcher can measure the degree to which the effect occurs at given ultrasound parameters, there is no simple link between these observed effects and a ‘representative size’

being activated unless the emulsions have very narrow distributions (which is difficult to achieve with nanoemulsions). Some have chosen to relate the activation parameters with distribution mean, median, or mode sizes, while others have found a high correlation with the larger content in the distribution (such as the 99th percentile size) (Fabiilli *et al.* 2009, Schad and Hynynen 2010, Zhang and Porter 2010, Reznik *et al.* 2011, Javadi *et al.* 2012, Lattin *et al.* 2012, Martin *et al.* 2012).

Thus, there is a need for methods that better assess the activation of PCCA nanoemulsions for studies of underlying physics and for defining practical *in vivo* parameters. We hypothesize that one method to achieve baseline measures of nanoemulsion activation for many formulations is to capture the distribution of bubbles generated by each ultrasound pulse and track how these distributions change with varying ultrasound pressure. This method of 'distribution-tracking' begins from the simple observation that individual droplets in a nanoemulsion cannot be measured optically, but the bubbles they produce once vaporized are typically on the order of 500 nm or larger – sufficient in size to resolve and measure on many optical systems (Sheeran *et al.* 2011b). By relating the microbubble size to the original droplet size by using modified ideal gas law relations, the changes in bubble distribution can be used to assess the efficiency of activating the originally nanoscale content of the emulsion. This also avoids the interfering effects of large outliers present in polydisperse populations: even though large content will be activated with high efficiency at a given pressure and result in very large bubbles, they will compose a very small portion of the distribution once the nanoscale content is being vaporized efficiently.

In order to use the bubble distribution resulting from an individual pulse as a measure of activation, it is essential to ensure that the droplet-to-bubble transition proceeds with minimal secondary effects – allowing the diameter of a bubble to be related to the originating droplet's size by ideal gas law relations. These secondary effects include the intake of ambient dissolved gases and interaction with subsequent ultrasound cycles in the vaporization pulse. Our previous study involving vaporization of decafluorobutane (DFB) microdroplets showed that even within a few seconds post-vaporization, the bubbles could be as much as twice the predicted size (Sheeran *et al.* 2011b) due to influx of dissolved gases. When the experiments were duplicated with degassed water, droplets expanded to very near the predicted size, and showed only minor growth over the course of several minutes. Therefore, we hypothesize that in order to assess activation by the bubbles produced, the experimental setup must be degassed, and the distributions must be captured shortly after vaporization. It is also possible that the distribution of bubbles resulting from a vaporization event will be influenced by the ultrasound pulse itself – although very little has been reported to this effect in PCCA literature to date. Even when formulated with highly volatile components, nanodroplet vaporization can require pressures significantly higher than what is commonly used for microbubble imaging (Rapoport *et al.* 2009b, Zhang and Porter 2010, Sheeran *et al.* 2011b, Sheeran *et al.* 2012). With high pressures and long pulse lengths comes an increased possibility for secondary effects such as microbubble destruction, fusion, and radiation-force interactions (Dayton *et al.* 1997, Postema *et al.* 2004). Therefore, we additionally hypothesize that in order to minimally effect the resulting bubble population, pulses as short as possible must be used to initiate vaporization. Though

long insonation periods at low amplitudes may ultimately cause droplet conversion by interaction with nearby bubbles produced earlier in the period (Lo *et al.* 2007) and/or by thermal means (Huang *et al.* 2010), activation by a pressure-only means is desired here.

In this study, we first investigate the influence of the vaporization pulse on the bubbles produced from DFB nanoemulsions through ultra-high-speed microscopy in order to determine the likelihood of secondary effects occurring within long vaporization pulses. We next demonstrate that *in vitro* activation of nanoemulsions by short pulses at several clinically relevant frequencies can be measured by tracking changes in the distribution of produced bubbles – providing practical *in vivo* activation parameters that optimally vaporize the nanoscale content at given frequencies and pulse lengths. Here, we consider droplet vaporization to be optimal when the majority of the bubbles produced originate from droplets forming the mode of the polydisperse size distribution. We further demonstrate that activation of low boiling point nanoscale PCCAs can be accomplished using pulse lengths and pressures within the output capabilities of common clinical ultrasound machines.

2. Methods

2.1.Decafluorobutane Nanodroplet Preparation

Polydisperse lipid-coated nanodroplets were prepared using a previously-described ‘microbubble condensation’ method that allows simple production of high-yield nanoemulsions from highly volatile compounds (Sheeran *et al.* 2011a, Sheeran *et al.* 2012). Briefly, polydisperse DFB microbubbles were formulated by a 9:1 M dissolution of 1,2-distearoyl-*sn*-glycero-3-phosphocholine (DSPC) and 1,2-distearoyl-*sn*-glycero-3-phosphoethanolamine-N-methoxy(polyethylene-glycol)-2000 (DSPE-PEG2000) for a total lipid concentration of 1 mg/mL (lipids purchased from Avanti Polar Lipids, Alabaster, AL) in an excipient solution of phosphate-buffered saline (PBS), propylene glycol, and glycerol (16:3:1). 1.5 mL of the lipid cocktail was added to a 3 mL glass vial, and the remaining headspace gas-exchanged with DFB (Fluoromed, Round Rock, TX). Standard mechanical agitation techniques (Vialmix, Bristol-Myers-Squibb, New York, NY) were used to generate a high-yield, polydisperse distribution of microbubbles within the vial. The resulting microbubble emulsions were allowed to cool to room temperature before being immersed in an isopropanol bath maintained between −7°C and −10°C and swirled gently for approximately 1 min. Though condensation was typically observed by this point (noted by a change in consistency and translucency), vials were then connected to an adjustable air-pressure source and the headspace pressure in the vial was increased (while the low temperature was maintained) to ensure the majority of particles reverted to the liquid state. The reduced freezing point of the emulsion as a result of the combination of propylene glycol, glycerol, and PBS prevented sample freezing during this process. Vials were then removed and stored at 4°C for up to 2 hours prior to use. Droplets were sized with dynamic light scattering (Malvern Nano ZS, Malvern Instruments Ltd., Malvern, Worcestershire, U.K.) by placing approximately 1.5 mL of a 10% dilution of the droplet emulsion in a plastic sizing cuvette. Nanodroplet emulsions yielded consistent size distributions with peaks on the order of 200 nm in diameter when weighted to either intensity or number, with a mean diameter on the order of 200–300 nm (figure 1).

2.2.Experimental Setup

The experimental setup used here was similar to that described in earlier studies (figure 2) (Sheeran *et al.* 2011b, Sheeran *et al.* 2011a, Sheeran *et al.* 2012). An acrylic-lined, continuously degassed water bath was maintained at 37°C and mounted onto an inverted microscope (Olympus IX71, Center Valley, PA). Images of bubble generation were captured using a 100x (NA = 1.0) water immersion objective interfaced with either an ultra-high-speed framing camera with a 24-frame buffer (SIMD24, Specialised Imaging, Simi Valley, CA) capable of imaging up to 200 million frames per second (for investigating activity within a single pulse), or a high-speed framing camera (FastCam SA1.1, Photron USA, Inc., San Diego, CA) set to 60 frames per second with a long buffer (for capturing bubbles generated after the pulse). For use with the ultra-high speed camera, a high intensity xenon strobe was interfaced with the microscope system to provide sufficient illumination. Otherwise, a standard 100-Watt halogen illuminator was used. Images and videos resulting from the experiments were analyzed using ImageJ software (NIH, Bethesda, MD). All optical measurements were calibrated by reticle. The practical optical resolution of the system limited measurement of particles to those greater than approximately 800 nm in diameter to maintain reasonable accuracy. For optical-acoustic alignment, the focus of the piston transducer used was positioned to be confocal with the microscope by use of a calibrated needle hydrophone (HNA-0400, Onda Corp., Sunnyvale, CA). Acoustic pulses were initiated by a manual trigger connected to the input of the high-speed camera in order to simultaneously capture video. Droplet solutions were pumped through a nearly optically and acoustically transparent 200 μm inner diameter microcellulose tube (Spectrum Laboratories, Inc., Greensboro, NC) using a custom-built manual volume injector that allowed the user to control the rate of flow, providing precise spatial manipulation of the volume being investigated. The portion of the tube resting in the confocal acoustic/optical plane was controlled by manipulating a 3-axis micro-positioner (MMO-203, Narishige Group, East Meadow, NY). While in the liquid state, droplets tended to settle toward the bottom of the tube, but once vaporized floated to the top due to buoyancy. By manipulating both the volume injector and the micropositioner, the entire volume of fluid being investigated before and after vaporization can be brought into focus and captured.

2.3.Acoustics

Three different ultrasound piston transducers were used in these studies to investigate the influence of frequency on droplet vaporization. In all cases, the piston transducers were driven by an arbitrary waveform generator signal (AFG 3101, Tektronix, Inc., Beaverton, OR) amplified 60 dB using an RF amplifier (A500, ENI, Rochester, NY). For ultra-high-speed imaging investigating activity within a single pulse, a 1 MHz center frequency spherically-focused transducer with a 2.2 cm diameter and focal length of 3.75 cm (IL0106HP, Valpey Fisher Corp., Hopkinton, MA) was driven with a 20-cycle sinusoid of adjustable amplitude at 1 MHz (total insonification time of 20 μs; approximately the maximum imaging time allowed by the flash bulb). The camera frame spacing was set to record at either 20 million frames per second with 30 ns exposure times to capture many frames within one cycle, or set to record at 1 million frames per second with 30 ns exposure to capture events occurring across several cycles. To capture bubble distributions in the

second set of experiments, the previously described 1 MHz transducer was used as well as transducers with 5 MHz (2.2 cm diameter, 5 cm focus; IL0506HP, Valpey Fisher Corp., Hopkinton, MA) and 7.5 MHz (2.2 cm diameter, 5 cm focus; V321, Panametrics, Inc., Waltham, MA) center frequencies. These transducers were driven using 2-cycle pulse excitation waveforms with variable amplitude at 1 MHz, 5.5 MHz, and 8 MHz, respectively. Because brief, high-intensity pulses typically in the non-linear regime were used, all transducers were calibrated at focus using a needle hydrophone (HNA-0400, Onda Corp., Sunnyvale, CA) with a magnitude-only hydrophone deconvolution method (Hurrell 2004).

2.4.Droplet Vaporization and Imaging of Bubble Distributions

During bubble distribution measurements, samples were diluted to between 10–30% in order to reduce the number of bubbles produced from each pulse (such that the majority of the bubbles weren't obscured from measurement by other bubbles). The droplet emulsions were injected via the custom volume injector and the forward flow stopped prior to initiation of the ultrasound pulse. The tube position relative to the acoustic/optical focus was adjusted so that the optical focus rested at an elevational plane approximately 70 μm from the microcellulose tube bottom (1/3 of the tube diameter). Once the ultrasound pulse was triggered manually, the tube was repositioned such that the focal plane was near the tube top, and several seconds were allowed to pass for bubbles to float to the focal plane. The micromanipulator was then used to translate through the tube elevationally and laterally to capture all bubbles present resulting from the single pulse. Staring from a lateral position downstream of the particle injection direction, the region of the tube in the optical focus was translated in a square-wave pattern along the lateral and elevational dimensions across the lateral length of the bubble cloud produced. This type of translation allowed resolution of bubbles beyond the microscope objective's depth of view. Between pulses, forward flow of the sample volume was restored in order to bring an unvaporized volume into the optical focus. Ultrasound parameters were selected by observing the lowest input parameters that repeatably generated a sufficient number of bubbles for measurement purposes (typically on the order of 30 bubbles per pulse), and 7 to 8 test pressures between this and the maximum output of each transducer were chosen. For each sample, the emulsion was either diluted to 30% in PBS (in order to produce larger number of bubbles at lower pressures where less activation is occurring) or 10% (in order to prevent obscuration of bubbles at higher pressures where high activation is occurring), and the bubbles emerging from each pulse recorded. Any bubble that was not stationary at the top of the tube was excluded, as well as any bubble with edges that could not be reasonably discerned. Bubbles from at least two pulses were captured at each test pressure (often 4–5 pulses for lower pressures) to ensure a sufficient number of bubble samples at each pressure were obtained. This process was repeated for 3 samples at each frequency (1 MHz, 5.5 MHz, 8 MHz).

2.5.Distribution Tracking Theory and Processing

A modified ideal gas law equation that includes the effects of Laplace pressure can be derived to predict the relationship between the expanded bubble and the originating droplet (Evans *et al.* 2006, Sheeran *et al.* 2011b):

$$r_l = \sqrt[3]{\frac{M r_g^3 (P + \frac{2\sigma}{r_g})}{\rho_l RT}} \quad (1)$$

where r_l is the radius of the liquid droplet, r_g is the radius of the gas microbubble, M is the molar mass, P is the ambient pressure, R is the ideal gas constant, T is the temperature, ρ_l is the liquid density, and σ is the surface tension. Here it is assumed that the number of moles is constant from the liquid state to the gas state. Using values reported earlier for DFB (Sheeran *et al.* 2011b) of M = 0.238 kg/mol, $\rho_l \approx 1500$ kg/m3, σ = 30 mN/m, and $P = P_{atm}$, the expansion of lipid-encapsulated DFB droplets originally 200 nm to 250 nm in diameter should result in microbubbles approximately 800 nm to 1.1 μm in diameter after vaporization. As the smallest size practically measureable in brightfield imaging is often on the order of 800 nm, tracking the bubble distribution that emerges after a vaporization event can provide substantial insight into the efficiency of vaporizing droplet distributions with peaks on the order of 200 nm in diameter or larger. In order for the resulting distributions to be accurate, however, any secondary effects such as bubble growth by intake of dissolved gasses, dissolution by gas exchange, and fusion or destruction by the ultrasound pulse must be minimized.

The concept of distribution tracking can be illustrated simply by assuming the DFB droplet distribution is Gaussian in nature, with a peak of 200 nm in diameter. By the ideal gas law relationship, if the emulsion is completely vaporized, the resulting mode bubble size would be 800 nm in diameter, which is large enough to capture by standard optical measures. Theoretically one could predict the resulting mean bubble size as well, though optical resolution limits would prevent experimentally recovering this (bubbles much smaller than 500 – 600 nm in diameter would not be visible or measurable). At a given ultrasound peak rarefactional pressure, the likelihood of vaporizing a droplet of a specific size is stochastic in nature, with the probability increasing as the droplet size increases (Sheeran and Dayton 2012). Thus, at low pressures, the upper tail of the distribution will constitute most of the droplet vaporization activity, with very little activation of smaller droplets. The resulting bubble distribution, in this case, will have a much larger mean and mode size than would be present for a highly optimized activation pulse. As the rarefactional pressure magnitude increases, the smaller emulsion droplets will vaporize with greater efficiency, and mode/mean sizes will continue to decrease. Once the peak in the droplet distribution begins to vaporize more efficiently, a transition will occur and the mode bubble size should remain stationary – as droplets smaller than this will produce fewer numbers of bubbles – though the mean will continue to decrease as the rarefactional pressure magnitude increases. As such, the interaction of the mean and mode bubble sizes as the pulse pressure increases should theoretically provide an indication of the peak droplet size activation.

In practice, there are experimental obstacles that prevent the ideal case from full realization. First, while the generation of droplets typically provides a uniform distribution, the ‘tails’ of the distribution are likely to be much more variable than a Gaussian distribution, and likely to be highly variable between samples, as this portion represents extreme outliers in the distribution. Therefore, statistics of the bubble distributions are expected to be highly

variable within samples and between samples until a significant portion of the main distribution (common to all samples) is being vaporized. Once the vaporization pulse is efficiently activating the main portion of the droplet distribution, these statistics should stabilize. Second, the optical resolution limits prevent continued tracking of the mode at sizes much smaller than 800 nm in diameter. With this limitation, once droplets that form bubbles on the order of 500 nm – 1 μm are being vaporized in significant numbers, the bubble distributions should still provide evidence of optimized activation (higher pressures will create a higher percentage of small bubbles; mean size will continue to decrease).

In these experiments, the area of all bubbles produced for an individual pulse that remained stationary in position near the top of the tube was measured by hand, converted to diameter, and collected in Excel. Within each emulsion sample, bubble measurements taken for a given ultrasound pressure across all pulses recorded were grouped so that the overall bubble distribution for each pressure could be assessed. All statistical outliers were removed from the measurements before statistics were calculated. The distribution mean and median were calculated from the resulting distribution. Samples were then rounded to the nearest 1 μm increment for calculation of the mode size such that bubbles on the order of 500 nm to 1.5 μm represented the smallest histogram bin. These measurements were repeated on all samples and the results averaged between samples to generate trends.

3. Results

3.1. Influence of Vaporization Pulse

Using 20-cycle pulses at 1 MHz, ultrasound parameters were increased gradually until they were observed to be sufficient to consistently vaporize DFB droplets into bubbles on the order of 1 – 5 μm in diameter. For these investigations into interactions within a single pulse, a peak rarefactional pressure of 1.45 MPa was found to be sufficient. In each case, the droplet emulsion was diluted to 50% in PBS. When set to record at 20 million frames per second, the vaporization activity within each single cycle could be visualized in high detail (figure 3). Near the trough of the first rarefactional half-cycle, non-visible nanodroplets began to vaporize (3b), resulting in a high number of bubbles visible within the focus that appeared to reach their maximal size within 150–200 ns of their vaporization (3d). As the transition to the compressional half-cycle began, all of the bubbles began to visibly compress and have disappeared from view completely by the peak of the compression (3g). In the sequential rarefactional trough, many of the previously visualized bubbles re-emerged, indicating they were not destroyed by the compression phase (3i), although many bubbles that were present in the first rarefactional cycle did not re-emerge, suggesting that each positive pressure phase has the potential to destroy some portion of the bubbles produced in the prior rarefactional phase. At these imaging and ultrasound parameters, this type of interaction between the resulting bubbles and the compression/rarefaction half-cycles was highly repeatable.

When recording at 1 million frames per second, vaporization activity across several cycles could be investigated. When the focus was kept approximately 70 μm from the tube bottom, some frames caught instances of the expansion/compression activity shown in figure 3, though the frame-rate was not high enough to capture in high detail. By re-focusing toward

the bottom of the tube where the large outlier droplets rested due to weight, vaporization of the very large droplets could be observed over several sequential cycles (figure 4). In the first compressional half-cycle, unvaporized droplets with diameters on the order of 1 – 5 μm could easily be resolved (4a), and began to vaporize in the first rarefactional half-cycle (not pictured). The much larger microscale droplets took longer to completely vaporize than the sub-micron droplets in figure 3, requiring on the order of 2 μs or more to fully expand, depending on size (see supplementary data). As they result from much larger droplets, these outliers of the distribution formed bubbles on the order of 5 μm in diameter or larger (much larger than those in figure 3). With the repeated sequence of compression/rarefaction, several phenomena previously noted for microbubbles (Postema *et al.* 2004) could be observed and were highly repeatable. During the rarefactional phase, fully expanded bubbles in close proximity could fuse and form larger bubbles (4b–d, white arrows), possibly as a result of over-expansion stretching the lipid membrane and allowing the gas interface of bubbles to come into contact. Over the course of several cycles, the bubbles were seen to cavitate violently, potentially causing jetting behavior, and move toward each other with each cycle due to secondary radiation force (c–i). Bubbles of this size were not destroyed by the ultrasound pulse as in figure 3, and as a result tended to fuse into a smaller number of larger bubbles over the course of the pulse. Images taken in this plane also highlight the complex, stochastic nature of droplet vaporization. Of the visible droplets (4a), the ones that ultimately vaporized in subsequent frames could not be predicted by size alone. In fact, one extreme outlier on the order of 5 μm in diameter could be visualized (4a, black arrow) that did not vaporize over several repeated rarefactional cycles, while much smaller droplets did vaporize. Whether this type of behavior is influenced by the complex acoustic field inside the tube (Kripfgans *et al.* 2004, Qin *et al.* 2008), or as a result of a mechanical coupling of the droplet to the tube as it rests at the bottom will require further investigation.

3.2.Bubble Distribution Tracking

In order to minimize the effects shown in the previous section, droplet emulsions diluted to between 10% and 30% (see Materials and Methods) were vaporized using short pulses at 1 MHz, 5.5 MHz, and 8 MHz (figure 5). Though the transducers were driven with a 2-cycle waveform, the bandwidth of the piston transducers resulted in additional ringing behavior that exposed droplets to additional compression and rarefactional cycles – most evident in the case of the 5.5 MHz transducer (5b).

As the ultrasound output increased, the overall number of bubbles produced also increased, and the number of bubbles on the order of 1 μm increased in proportion – indicating greater efficiency of vaporizing the non-visible nanodroplets (figure 6). At the lowest pressures tested, bubbles tended to be on the order of 5 μm or larger in diameter (6a), while at the highest pressures used the majority of bubbles present were near 1 μm in diameter (6b). It is worth noting that the lowest ultrasound output used was not a lower limit of vaporization, but that it produced enough bubbles to simplify distribution measurements. It is highly likely that some droplet vaporization is occurring at pressures below these, though it is not likely to be primarily from the nanoscale content.

The diameter of all bubbles in focus post-vaporization for each sample at the test pressures used were analyzed from images such as figure 6. In order to ensure the fidelity of the conclusions, a high number of bubbles were counted for each sample – approximately 3,200 bubbles per sample (or 9,700 total sizings for each frequency). The total number of bubbles sized over all experiments was nearly 30,000.

As is common with phase-change contrast agents involving low boiling point perfluorocarbons, some degree of spontaneous bubble generation is present. In these experiments, bubbles present without exposure to ultrasound were observed very sparsely, and were typically not present in the optical focus at the time of insonation. Videos of these bubbles in three control DFB droplet samples (not exposed to ultrasound) were sized, and showed that without ultrasound, bubbles present in solution (N = 610) had mean diameters of 8.6 ± 3.3 μm, with a mode of approximately 3 μm (figure 7).

Bubbles resulting from vaporization pulses were analyzed (as described in Materials and Methods) with regard to mean, median, and mode bubble diameter at each pressure in order to ascertain trends occurring with increasing acoustic parameters, and averaged across all samples at each frequency (figure 8). In general, mean bubble size at the lowest ultrasound pressure used in each case tended to be 7 – 8 μm in size, and decreased significantly ($p<0.01$) to a mean between 4 – 5 μm at the highest ultrasound pressure used (8a) due to the increase in the number of small bubbles at higher pressures. Median size showed virtually identical trends as mean size, and is not shown here. Like the mean size, the mode of the bubble distribution was on the order of 7 – 9 μm in diameter at lower ultrasound output (8b). As expected, high variation in the mode size at low pressures was observed between samples. As ultrasound output increased with each frequency, the mode generally decreased with high variation until settling at 1 μm, the smallest bin used. Past this transition, the mode remained stable at all higher output pressures, and the difference in the measurements at the highest output for each frequency were highly significant compared to the lowest output pressures ($p << 0.01$).

These results also show that, even when driving parameters were relatively similar, frequency of the incident ultrasound pulse appeared to play a role in the pressures required for vaporization. At the lowest ultrasound frequency used, significant bubble formation was noted at rarefactional pressures as low as 1 MPa, while at 8 MHz, the same distribution of bubbles was not present until rarefactional pressure reached approximately 3 MPa. Similarly, the mode size for 1 MHz ultrasound appeared to reach its final value at rarefactional pressures near 2 – 2.25 MPa, while this transition did not occur for 8 MHz ultrasound until rarefactional pressures near 3.75 MPa. In each case, the 5.5 MHz ultrasound characteristics were in between those obtained with 1 MHz and 8 MHz ultrasound.

4. Discussion

4.1. Vaporization Pulse

Some prior studies have explored the dynamics of dodecafluoropentane microdroplet vaporization on a short timescale and noted instances of complex vaporization behavior. In particular, Wong *et al.* (2011) showed that bubble evolution may proceed in stages after

initial nucleation, while Haworth and Kripfgans (2008) demonstrated that longer pulse lengths increased the probability of an individual microdroplet vaporizing and reported instances of coalescence of bubbles in close proximity. Reznik *et al.* (2013) recently demonstrated sub-micron agents may recondense back to the liquid state after vaporization, but that coalescence of bubbles increased the chance of bubble survival. Finally, Shpak *et al.* (2013) revealed that pulse length and frequency can significantly affect the rate at which bubble evolution occurs in the initial stages, and that, depending on the extent of inward gas diffusion, DDFP vapor bubbles may re-condense within the pulse compression phase. Similarly, the results reported here demonstrate preliminary evidence that bubbles produced early in the pulse can be significantly affected by the ultrasound pulse itself through destruction or coalescence, and that these types of interactions increase with pulse length. For many therapeutic applications, such as cavitation enhancement, this type of acoustic activity may be acceptable and/or desired. Haworth and Kripfgans (2008) suggest coalescence may be useful for applications such as vessel occlusion, but not for others such as phase aberration correction. For applications that seek to generate a large number of bubbles for contrast while minimizing bubble-induced bioeffects, a better understanding of these types of effects is needed. It may be that small bubbles are more likely to be destroyed by compression, while the large bubbles resist destruction by compression and are more likely to fuse and form larger bubbles. The precise interplay between droplet activation and the rarefaction/compression cycles may not be simply that more cycles will produce more bubbles, but that there is a balance between maximizing bubbles produced from the rarefactional phase, and minimizing secondary effects caused by the compression phase. Effects such as these are also sources of skew when measuring droplet activation through echogenicity or echo amplitude produced.

4.2.Optimizing Activation via Distribution Tracking

Aside from the sources of error presented above (selective bubble destruction/fusion), other effects do influence the accuracy of distribution tracking. Because larger bubbles are much more buoyant than very small bubbles, it is expected that some of the small bubbles were obscured by large bubbles in the optical focus. Additionally, the very small bubbles were more subject to the inertial forces of the surrounding fluid, and were often seen to be translating laterally just beyond the focal plane. Because the criterion for measurement was that the bubbles were stationary at the top of the tube, both of these effects resulted in a possible skew towards larger bubbles in the measurements. Any gas-exchange that may have occurred between vaporization and data collection would also have resulted in a skew towards a larger distribution, although this was limited by degassing the experimental setup. As such, the trends reported may be overestimates of the actual pressures needed to result in the distribution produced.

The changes in the bubble distributions as a function of ultrasound pressure can be illustrated clearly by combining all of the sizings obtained over all samples for an individual frequency (figure 9). Once ultrasound pressure is high enough to cause bubble generation, the main lobe of the distribution at first shifts to values much higher than the spontaneous control bubbles (figure 7), and only a small portion of the distribution is represented by the smallest bin size. As pressure increases, the peak of the main lobe begins to decrease, and

the number of very small bubbles increases until it becomes the peak of the distribution – now much lower than the control values. As pressure continues to increase, this peak increases in proportion to the rest of the distribution, indicating greater efficiency of vaporization.

Many multi-variable metrics can be chosen in order to capture the dynamic changes in bubble distribution occurring as a function of rarefactional pressure, such as Wasserstein metrics (Givens and Shortt 1984) or other more basic measures of histogram skew (Groeneveld and Meeden 1984). In this study, we demonstrate this through use of Pearson's first skewness coefficient (Pearson's mode) in order to combine several aspects of figure 8 into one measure:

$$skew = \frac{(mean - mode)}{std\ dev} \quad (2)$$

Theoretically, when pressures are low, both the mean and the mode should be relatively large and of similar value (although high variability is expected), and so skew should be near zero. As activation of smaller droplets becomes more efficient, the mode will shift rapidly, while the mean shifts gradually, causing a sharp increase in the skew measure. Once the mode settles, the mean will continue to decrease slowly, resulting in a gradual decrease of the skew. Using this measure on the previously presented distribution data, and averaging across the samples at each frequency, a clear picture of the transition can be obtained (figure 10). As expected, the variability at low pressures for each frequency is relatively high, and compounded by the combination of variation in mean and mode, but the skew peaks at a transitional pressure and remains constant or decreases slightly past this.

The skew analysis further demonstrates the relationship between frequency and droplet vaporization – that under these experimental parameters, the pressure required to activate nanodroplets increased with ultrasound frequency. The transitional pressure past which a similar distribution skew was achieved occurred near 2 MPa for 1 MHz, near 3 MPa for 5.5 MHz, and near 3.75 MPa for 8 MHz. Figure 5 demonstrates the pressure waveforms when driven at pressures near the transition points in figure 10. One would initially expect that the 5.5 MHz transition pressure would occur nearer to the pressure required at 8 MHz than 1 MHz. However, the low bandwidth of the 5.5 MHz transducer resulted in many more additional ultrasound cycles (figure 5b) that may have reduced the pressures needed to obtain similar distributions.

These results contradict an early and longstanding view in the PCCA literature that the pressures needed to achieve droplet vaporization can be reduced by increasing the ultrasound frequency (Kripfgans *et al.* 2000, Kripfgans *et al.* 2002, Schad and Hynynen 2010, Williams *et al.* 2013), although recent studies (including this one) have found the contrary to be true (Martin *et al.* 2012). As Reznik *et al.* (2011) have pointed out, an inverse relationship between frequency and vaporization pressure is not predicted by homogeneous nucleation theory, and so more understanding on the link between the two is needed. The current FDA guidelines for maximum pressure output on a diagnostic machine in soft tissue is a mechanical index (defined as the derated peak negative pressure in MPa divided by the

square root of the ultrasound frequency in MHz) of 1.9. For this study, this corresponds to peak negative pressures of 1.9 MPa, 4.5 MPa, and 5.4 MPa for 1 MHz, 5.5 MHz, and 8 MHz, respectively. It's worth noting, however, that even though the threshold pressures reported here do not appear to decrease with increasing frequency, the mechanical index needed does decrease with ultrasound frequency – which is important for *in vivo* implementation in many cases.

Part of the contradiction in the literature may be as a result of the type of measurement (most reporting this trend use phenomenological measures based on echo amplitude), but also may be due to variation in choice of ultrasound parameters at different frequencies, such as whether to match total pulse length or number of cycles. Matching the total pulse length results in a similar exposure time, but means that droplets at higher frequencies will experience significantly more compression/rarefaction cycles - likely influencing the probability of an individual droplet vaporizing. In this study, unlike many that report the inverse frequency/pressure relationship, we chose to match the number of compression/rarefaction cycles in short bursts as closely as possible in order to minimize secondary effects. With these parameters, the increase in pressure needed with increasing frequency may be partly explained by the beam width of the transducer itself. According to Cobbold (2007), the lateral and axial full-width half-max of the pressure field delivered from a concave piston are approximated as:

$$FWHM_{lat} = \frac{1.4\lambda Z_f}{D} \quad (3)$$

$$FWHM_{ax} = 7.2\lambda\left(\frac{Z_f}{D}\right)^2 \quad (4)$$

where λ is the wavelength, Z_f is the radial distance to the focus, and D is the transducer diameter. With the transducers used, the theoretical lateral FWHM was 3.60 mm, 0.90 mm, and 0.62 mm, for 1 MHz, 5.5 MHz, and 8 MHz, respectively, while the axial FWHM was 18.7 mm, 4.6 mm, and 3.2 mm, respectively. Because the microcellulose tube only measured 200 μm in diameter, the difference in the axial beam width between the frequencies likely played little role. However, the bubble cloud generated inside the tube typically spanned 1 mm or more laterally, and so the lateral beam width likely played a high role in the difference between frequencies. In other words, in order to create a similar distribution of bubbles between 8 MHz and 1 MHz, it may be that the peak rarefactional pressure at 8 MHz needed to be much larger in order to compensate for the rapid pressure drop-off laterally and make the FWHM pressure comparable. Because the transition threshold measured by bubble distribution tracking takes into account aspects such as these, these thresholds are likely to correlate to appropriate *in vivo* pressures – where it is more desirable that a spatial extent of droplets is vaporized rather than a few droplets precisely at the peak in the pressure field.

These results should be used as a guide to what *in vivo* pressures would be necessary for very short pulses (such as implementation of vaporization pulses on diagnostic arrays) in order to minimize bioeffects introduced by longer pulses, but they can also be used as a

baseline for other measurements. For example, if gauging appropriate acoustic parameters for activation using a phenomenological method such as release of dye, one could first use distribution tracking to assess the relationship between bubble formation and dye release using short pulses of varying pressure in order to achieve a baseline. Then the researcher could increase the acoustic conditions (pulse length, pulse repetition frequency, etc…) and observe the change in the phenomenological effect.

There are certain PCCA formulations where distribution tracking may not be applicable. Several researchers have suggested that droplets composed of higher boiling point perfluorocarbons may be useful in that they could re-condense immediately after the vaporization pulse ends, and can be made to undergo phase-transition several times (Rapoport *et al.* 2011). In this case, measuring the bubble distribution after the pulse ends would be impossible. Additionally, droplet formulations with high monodispersity, which are often found with microscale droplets in microfluidics-based approaches (Couture *et al.* 2011, Bardin *et al.* 2011, Martz *et al.* 2011), would not benefit from this method, as the activation would be highly uniform across the entire distribution. Finally, nanoemulsions where the peak diameter lies on the order of 100 nm or less would produce bubbles too small to be optically observed and measured. Though this would prevent a distribution tracking method, the bubbles produced would be echogenic and could be measured via more commonly-used echo amplitude methods.

5. Summary

Based on these methods, we have shown that vaporization of decafluorobutane droplets in the 200 nm diameter range can be achieved using very short pulses with pressures relevant to diagnostic use. With a given ultrasound frequency and pulse length, pressure required for vaporization of the distribution's modal peak can be gauged by observing changes in the bubble population produced with each pulse as pressure is increased. We additionally show that further understanding is needed of the impact of long vaporization pulses, which may selectively destroy or fuse bubbles produced in early cycles.

Supplementary Material

Refer to Web version on PubMed Central for supplementary material.

Acknowledgment

This work was supported in part by NIH grants no. EB-011704, and EB-008733 as well as pilot funds from National Science Foundation, DMR#1122483, and the Carolina Center for Cancer Nanotechnology Excellence. The high speed imaging system was purchased through NIH shared instrumentation grant S10 RR025594. The authors would like to thank Ali Dhanaliwala and Professor John Hossack at the University of Virginia for assistance with ultra-high-speed imaging, Ryan Gessner for discussions involving distribution statistics, and Steven Feingold for setup assistance and manuscript edits. P.S. appreciates the generous support of the National Science Foundation as the recipient of a graduate fellowship.

References

Bardin D, Martz TD, Sheeran PS, Shih R, Dayton PA, Lee AP. High-speed, clinical-scale microfluidic generation of stable phase-change droplets for gas embolotherapy. Lab Chip. 2011; 11:3990–3998. [PubMed: 22011845]

Brennen, CE. Cavitation and Bubble Dynamics. Oxford, New York: Oxford University Press; 1995.

Campbell RB. Tumor physiology and delivery of nanopharmaceuticals. Anticancer Agents Med Chem. 2006; 6:503–512. [PubMed: 17100555]

Cobbold, RSC. Foundations of biomedical ultrasound. New York, New York: Oxford University Press; 2007.

Couture O, Faivre M, Pannacci N, Babataheri A, Servois V, Tabeling P, Tanter M. Ultrasound internal tattooing. Medical Physics. 2011; 38:1116–1123. [PubMed: 21452748]

Couture O, Urban A, Bretagne A, Martinez L, Tanter M, Tabeling P. In vivo targeted delivery of large payloads with an ultrasound clinical scanner. Med Phys. 2012; 39:5229–5237. [PubMed: 22894447]

Dayton PA, Morgan KE, Klibanov AL, Brandenburger G, Nightingale KR, Ferrara KW. A preliminary evaluation of the effects of primary and secondary radiation forces on acoustic contrast agents. Ultrasonics, Ferroelectrics and Frequency Control, IEEE Transactions on. 1997; 44:1264–1277.

Evans DR, Parsons DF, Craig VSJ. Physical properties of phase-change emulsions. Langmuir. 2006; 22:9538–9545. [PubMed: 17073477]

Fabiilli M, Lee J, Kripfgans O, Carson P, Fowlkes J. Delivery of Water-Soluble Drugs Using Acoustically Triggered Perfluorocarbon Double Emulsions. Pharmaceutical Research. 2010a; 27:2753–2765. [PubMed: 20872050]

Fabiilli ML, Haworth KJ, Fakhri NH, Kripfgans OD, Carson PL, Fowlkes JB. The role of inertial cavitation in acoustic droplet vaporization. Ultrasonics, Ferroelectrics and Frequency Control, IEEE Transactions on. 2009; 56:1006–1017.

Fabiilli ML, Haworth KJ, Sebastian IE, Kripfgans OD, Carson PL, Fowlkes JB. Delivery of Chlorambucil Using an Acoustically-Triggered Perfluoropentane Emulsion. Ultrasound in Medicine & Biology. 2010b; 36:1364–1375. [PubMed: 20691925]

Giesecke T, Hynynen K. Ultrasound-mediated cavitation thresholds of liquid perfluorocarbon droplets in vitro. Ultrasound Med Biol. 2003; 29:1359–1365. [PubMed: 14553814]

Givens CR, Shortt RM. A class of Wasserstein metrics for probability distributions. The Michigan Mathematical Journal. 1984; 31:231–240.

Gramiak R, Shah PM. Echocardiography of the aortic root. Invest Radiol. 1968; 3:356–366. [PubMed: 5688346]

Groeneveld RA, Meeden G. Measuring skewness and kurtosis. The Statistician. 1984; 33:391–399.

Haworth KJ, Fowlkes JB, Carson PL, Kripfgans OD. Towards Aberration Correction of Transcranial Ultrasound Using Acoustic Droplet Vaporization. Ultrasound in Medicine & Biology. 2008; 34:435–445. [PubMed: 17935872]

Haworth, KJ.; Kripfgans, OD. Initial growth and coalescence of acoustically vaporized perfluorocarbon microdroplets Ultrasonics Symposium, 2008. IUS 2008; IEEE. 2–5 Nov; 2008. p. 623-626.

Huang J, Xu JS, Xu RX. Heat-sensitive microbubbles for intraoperative assessment of cancer ablation margins. Biomaterials. 2010; 31:1278–1286. [PubMed: 19942283]

Hurrell A. Voltage to pressure conversion: are you getting `phased' by the problem? Journal of Physics: Conference Series. 2004; 1:57.

Javadi M, Pitt WG, Belnap DM, Tsosie NH, Hartley JM. Encapsulating nanoemulsions inside eLiposomes for ultrasonic drug delivery. Langmuir. 2012; 28:14720–14729. [PubMed: 22989347]

Kawabata K-I, Sugita N, Yoshikawa H, Azuma T, Umemura S-I. Nanoparticles with multiple perfluorocarbons for controllable ultrasonically induced phase shifting. Jpn. J. Appl. Phys. 2005; 44:5.

Kripfgans OD, Fabiilli ML, Carson PL, Fowlkes JB. On the acoustic vaporization of micrometer-sized droplets. The Journal of the Acoustical Society of America. 2004; 116:272–281. [PubMed: 15295987]

Kripfgans OD, Fowlkes JB, Miller DL, Eldevik OP, Carson PL. Acoustic droplet vaporization for therapeutic and diagnostic applications. Ultrasound in Medicine & Biology. 2000; 26:1177–1189. [PubMed: 11053753]

Kripfgans OD, Fowlkes JB, Woydt M, Eldevik OP, Carson PL. In vivo droplet vaporization for occlusion therapy and phase aberration correction. Ultrasonics, Ferroelectrics and Frequency Control, IEEE Transactions on. 2002; 49:726–738.

Kripfgans OD, Orifici CM, Carson PL, Ives KA, Eldevik OP, Fowlkes JB. Acoustic droplet vaporization for temporal and spatial control of tissue occlusion: a kidney study. Ultrasonics, Ferroelectrics and Frequency Control, IEEE Transactions on. 2005; 52:1101–1110.

Lattin JR, Pitt WG, Belnap DM, Husseini GA. Ultrasound-Induced Calcein Release From eLiposomes. Ultrasound in Medicine & Biology. 2012; 38:2163–2173. [PubMed: 23062373]

Lo AH, Kripfgans OD, Carson PL, Fowlkes JB. Spatial control of gas bubbles and their effects on acoustic fields. Ultrasound in Medicine & Biology. 2006; 32:95–106. [PubMed: 16364801]

Lo AH, Kripfgans OD, Carson PL, Rothman ED, Fowlkes JB. Acoustic droplet vaporization threshold: effects of pulse duration and contrast agent. Ultrasonics, Ferroelectrics and Frequency Control, IEEE Transactions on. 2007; 54:933–946.

Martin AL, Seo M, Williams R, Belayneh G, Foster FS, Matsuura N. Intracellular growth of nanoscale perfluorocarbon droplets for enhanced ultrasound-induced phase-change conversion. Ultrasound Med Biol. 2012; 38:1799–1810. [PubMed: 22920544]

Martin KH, Dayton PA. Current status and prospects for microbubbles and ultrasound theranostics. WIREs Nanomed Nanobiotechnol. 2013

Martz TD, Sheeran PS, Bardin D, Lee AP, Dayton PA. Precision Manufacture of Phase-Change Perfluorocarbon Droplets Using Microfluidics. Ultrasound in Medicine & Biology. 2011; 37:1952–1957. [PubMed: 21963036]

Miller DL, Kripfgans OD, Fowlkes JB, Carson PL. Cavitation nucleation agents for nonthermal ultrasound therapy. The Journal of the Acoustical Society of America. 2000; 107:3480–3486. [PubMed: 10875392]

Miller DL, Song J. Lithotripter shock waves with cavitation nucleation agents produce tumor growth reduction and gene transfer in vivo. Ultrasound in Medicine & Biology. 2002; 28:1343–1348. [PubMed: 12467861]

Phillips LC, Puett C, Sheeran PS, Miller GW, Matsunaga TO, Dayton PA. Phase-shift perfluorocarbon agents enhance high intensity focused ultrasound (HIFU) thermal delivery with reduced near-field heating. J Acoust Soc Am. 2013; 134:1473–1482. [PubMed: 23927187]

Postema M, Van Wamel A, Lancée CT, De Jong N. Ultrasound-induced encapsulated microbubble phenomena. Ultrasound in Medicine & Biology. 2004; 30:827–840. [PubMed: 15219962]

Qin S, Kruse DE, Ferrara KW. Transmitted Ultrasound Pressure Variation in Micro Blood Vessel Phantoms. Ultrasound in Medicine & Biology. 2008; 34:1014–1020. [PubMed: 18395962]

Rapoport N. Phase-shift, stimuli-responsive perfluorocarbon nanodroplets for drug delivery to cancer. WIREs Nanomed Nanobiotechnol. 2012; 4:492–510.

Rapoport N, Nam K-H, Gupta R, Gao Z, Mohan P, Payne A, Todd N, Liu X, Kim T, Shea J, Scaife C, Parker DL, Jeong E-K, Kennedy AM. Ultrasound-mediated tumor imaging and nanotherapy using drug loaded, block copolymer stabilized perfluorocarbon nanoemulsions. Journal of Controlled Release. 2011; 153:4–15. [PubMed: 21277919]

Rapoport NY, Efros AL, Christensen DA, Kennedy AM, Nam KH. Microbubble Generation in Phase-Shift Nanoemulsions used as Anticancer Drug Carriers. Bubble Sci Eng Technol. 2009a; 1:31–39. [PubMed: 20046899]

Rapoport NY, Kennedy AM, Shea JE, Scaife CL, Nam KH. Controlled and targeted tumor chemotherapy by ultrasound-activated nanoemulsions/microbubbles. J Control Release. 2009b; 138:268–276. [PubMed: 19477208]

Reznik N, Seo M, Williams R, Bolewska-Pedyczak E, Lee M, Matsuura N, Gariepy J, Foster FS, Burns PN. Optical studies of vaporization and stability of fluorescently labelled perfluorocarbon droplets. Physics in Medicine and Biology. 2012; 57:7205. [PubMed: 23060210]

Reznik N, Shpak O, Gelderblom E, Williams R, De Jong N, Versluis M, Burns PN. The efficiency and stability of bubble formation by acoustic vaporization of submicron perfluorocarbon droplets. Ultrasonics. 2013

Reznik N, Williams R, Burns PN. Investigation of Vaporized Submicron Perfluorocarbon Droplets as an Ultrasound Contrast Agent. Ultrasound in Medicine & Biology. 2011; 37:1271–1279. [PubMed: 21723449]

Schad KC, Hynynen K. In vitro characterization of perfluorocarbon droplets for focused ultrasound therapy. Phys Med Biol. 2010; 55:4933–4947. [PubMed: 20693614]

Sheeran PS, Dayton PA. Phase-change contrast agents for imaging and therapy. Current pharmaceutical design. 2012; 18:2152–2165. [PubMed: 22352770]

Sheeran PS, Luois S, Dayton PA, Matsunaga TO. Formulation and acoustic studies of a new phase-shift agent for diagnostic and therapeutic ultrasound. Langmuir. 2011a; 27:10412–10420. [PubMed: 21744860]

Sheeran PS, Luois SH, Mullin LB, Matsunaga TO, Dayton PA. Design of ultrasonically-activatable nanoparticles using low boiling point perfluorocarbons. Biomaterials. 2012; 33:3262–3269. [PubMed: 22289265]

Sheeran PS, Streeter JE, Mullin LB, Matsunaga TO, Dayton PA. Toward ultrasound molecular imaging with phase-change contrast agents: An in-vitro proof-of-principle. Ultrasound Med Biol. 2013; 39:893–902. **In Press.** [PubMed: 23453380]

Sheeran PS, Wong VP, Luois S, Mcfarland RJ, Ross WD, Feingold S, Matsunaga TO, Dayton PA. Decafluorobutane as a phase-change contrast agent for low-energy extravascular ultrasonic imaging. Ultrasound in Medicine & Biology. 2011b; 37:1518–1530. [PubMed: 21775049]

Shpak O, Stricker L, Versluis M, Lohse D. The role of gas in ultrasonically driven vapor bubble growth. Phys Med Biol. 2013; 58:2523–2535. [PubMed: 23528293]

Stride EP, Coussios CC. Cavitation and contrast: the use of bubbles in ultrasound imaging and therapy. Proceedings of the Institution of Mechanical Engineers, Part H: Journal of Engineering in Medicine. 2010; 224:171–191.

Strohm E, Rui M, Gorelikov I, Matsuura N, Kolios M. Vaporization of perfluorocarbon droplets using optical irradiation. Biomed. Opt. Express. 2011; 2:1432–1442. [PubMed: 21698007]

Strohm EM, Gorelikov I, Matsuura N, Kolios MC. Acoustic and photoacoustic characterization of micron-sized perfluorocarbon emulsions. Journal of Biomedical Optics. 2012; 17:096016–096011.

Wang C-H, Kang S-T, Lee Y-H, Luo Y-L, Huang Y-F, Yeh C-K. Aptamer-conjugated and drug-loaded acoustic droplets for ultrasound theranosis. Biomaterials. 2012a; 33:1939–1947. [PubMed: 22142768]

Wang C-H, Kang S-T, Yeh C-K. Superparamagnetic iron oxide and drug complex-embedded acoustic droplets for ultrasound targeted theranosis. Biomaterials. 2012b; 34:1852–1861. [PubMed: 23219326]

Williams R, Wright C, Cherin E, Reznik N, Lee M, Gorelikov I, Foster FS, Matsuura N, Burns PN. Characterization of Submicron Phase-change Perfluorocarbon Droplets for Extravascular Ultrasound Imaging of Cancer. Ultrasound in Medicine & Biology. 2013; 39:475–489. [PubMed: 23312960]

Wilson K, Homan K, Emelianov S. Biomedical photoacoustics beyond thermal expansion using triggered nanodroplet vaporization for contrast-enhanced imaging. Nat Commun. 2012; 3:618. [PubMed: 22233628]

Wong ZZ, Kripfgans OD, Qamar A, Fowlkes JB, Bull JL. Bubble evolution in acoustic droplet vaporization at physiological temperature via ultra-high speed imaging. Soft Matter. 2011; 7:4009–4016.

Zhang M, Fabiilli ML, Haworth KJ, Fowlkes JB, Kripfgans OD, Roberts WW, Ives KA, Carson PL. Initial Investigation of Acoustic Droplet Vaporization for Occlusion in Canine Kidney. Ultrasound in Medicine & Biology. 2010; 36:1691–1703. [PubMed: 20800939]

Zhang M, Fabiilli ML, Haworth KJ, Padilla F, Swanson SD, Kripfgans OD, Carson PL, Fowlkes JB. Acoustic Droplet Vaporization for Enhancement of Thermal Ablation by High Intensity Focused Ultrasound. Acad Radiol. 2011; 18:1123–1132. [PubMed: 21703883]

Zhang P, Porter T. An in vitro study of a phase-shift nanoemulsion: a potential nucleation agent for bubble-enhanced HIFU tumor ablation. Ultrasound Med Biol. 2010; 36:1856–1866. [PubMed: 20888685]

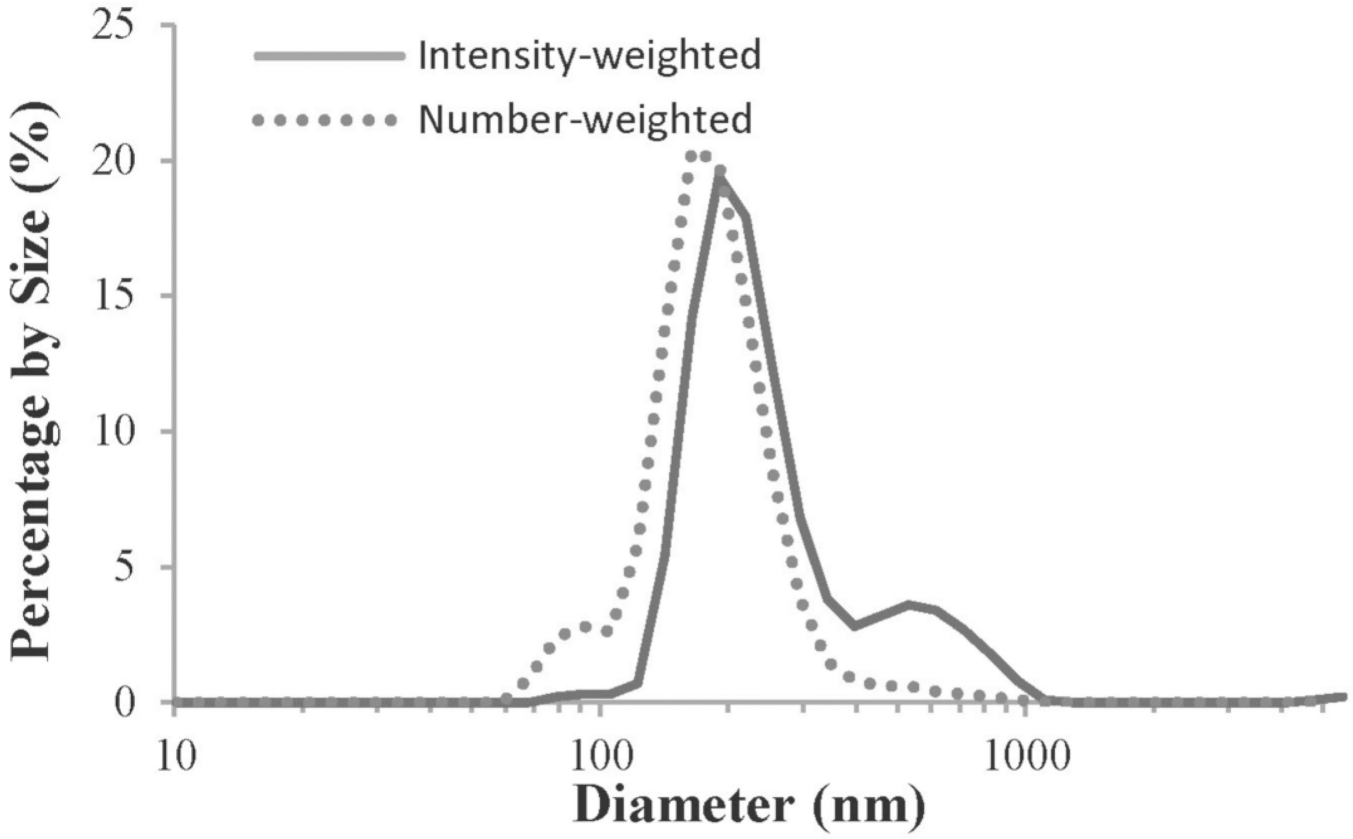

Figure 1.

Dynamic light scattering measurements of DFB nanoemulsions produced by microbubble condensation. Lines show the result of sizing averaged for 3 repeated measurements per sample over 3 samples (9 total measurements), in both a number-weighted and intensity-weighted format. When number-weighted, the mode diameter occurs at 164 nm, with a mean droplet diameter of 192 ± 85 nm; when intensity-weighted, mode size occurs at 190 nm with mean size of 297 ± 323 nm. *Note: Malvern Nano ZS set to 'Multiple Narrow Modes' for high-resolution analysis.*

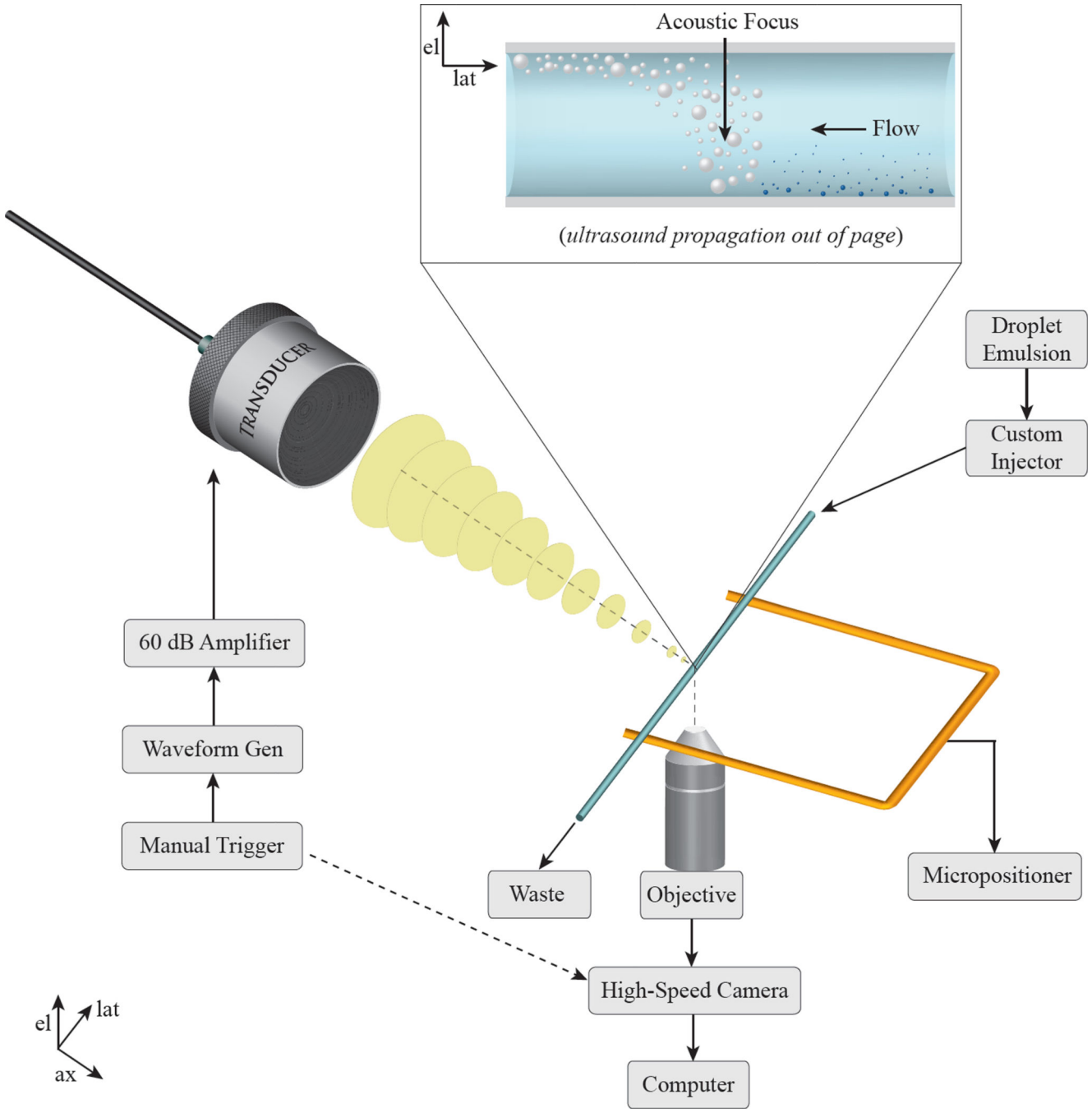

Figure 2.

Experimental setup. A piston ultrasound transducer is manually triggered to deliver a short pulse to the portion of the microcellulose tube resting in the optical plane. Prior to droplet vaporization, large droplets can be visualized near the bottom of the tube with no significant presence of bubbles near the top of the tube. After vaporization is induced, the focal plane is adjusted to the top of the microcellulose tube to capture images of bubbles produced. Axes indicate the elevational, lateral, and axial dimensions of the incident ultrasound pulse.

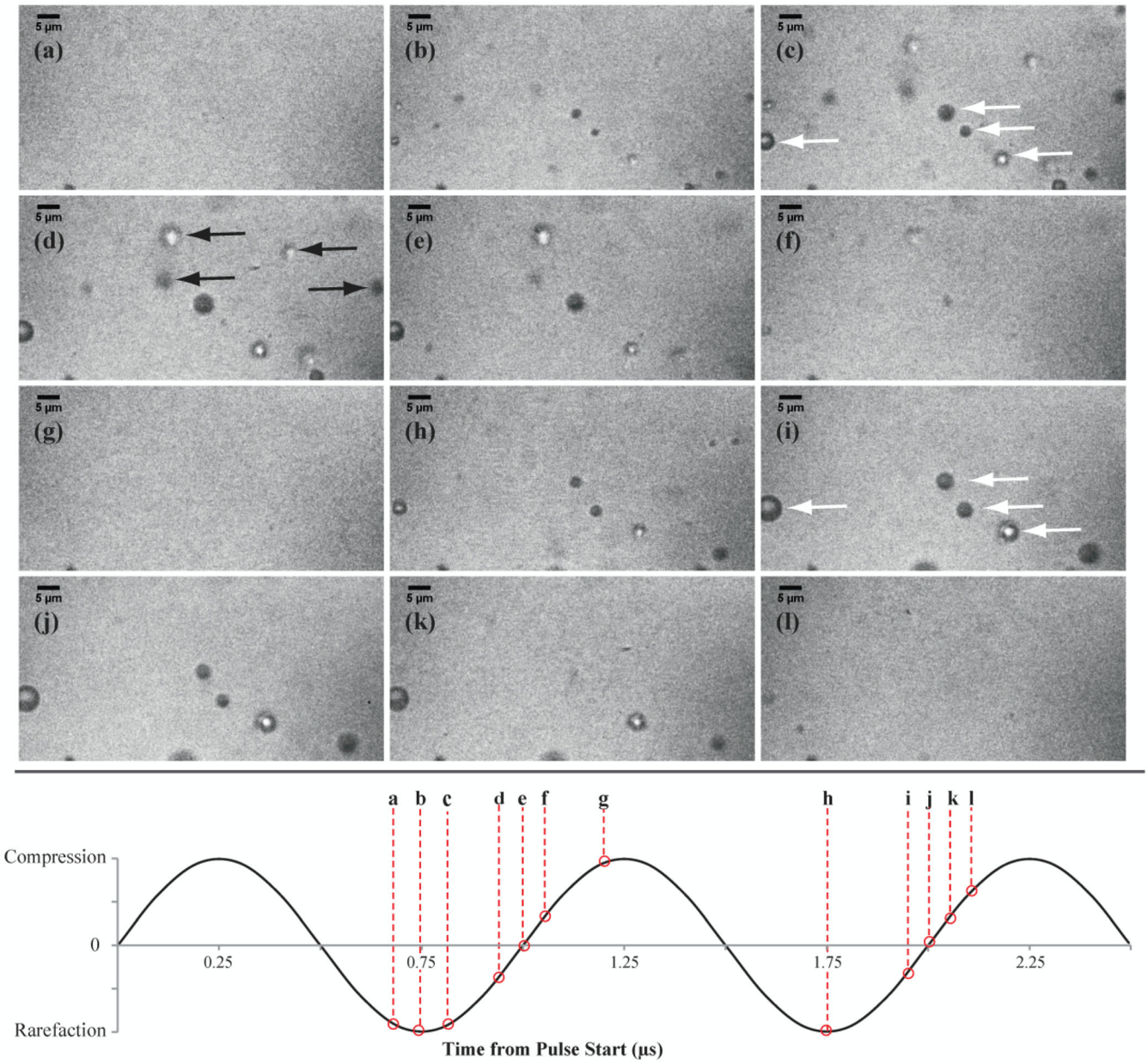

Figure 3.

Ultra-high-speed microscopy (20 million frames per second) of bubbles produced during a 1 MHz, 20-cycle vaporization pulse of 1.45 MPa rarefactional pressure. Many bubbles are observed to emerge through the first rarefactional phase (a–d), but as the transition through the second compression phase occurs (e–g) the bubbles are observed to compress and disappear from view. Upon the second rarefactional phase (h,i), many of the bubbles re-emerge (denoted by white arrows), but those indicated by black arrows in (d) do not re-appear. During the third compression phase (j – i), the bubbles are observed to compress again. Scale bars indicate 5 µm. *Note: This image comprises 12 selected frames from a longer source video. See Supplemental Data for source video.*

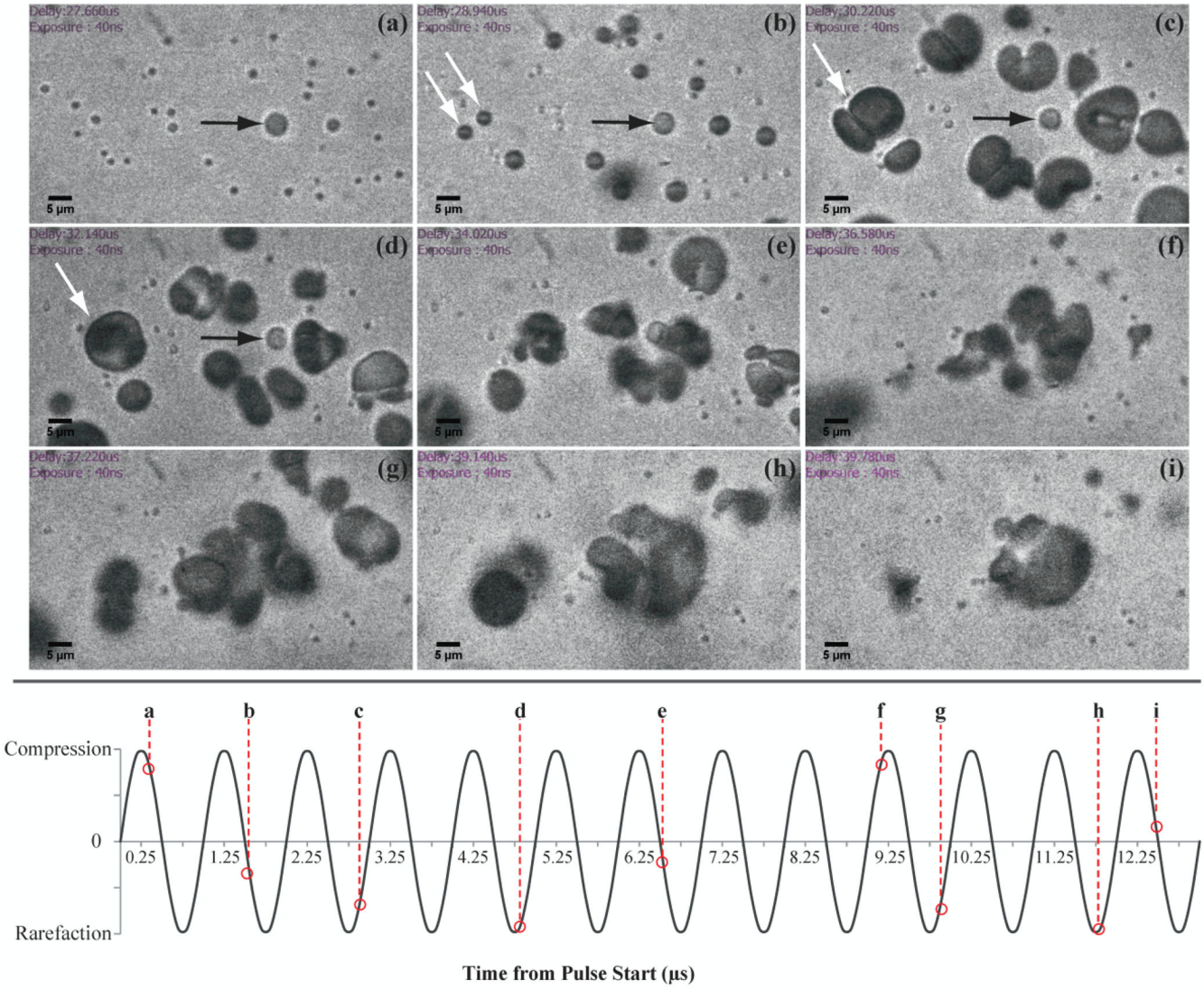

Figure 4.

Ultra-high-speed microscopy (1 million frames per second) of bubbles produced during a 1 MHz, 20-cycle vaporization pulse of 1.45 MPa rarefactional pressure. Droplets are observed to vaporize in the first rarefactional phases and fully expand within 1–2 µs (a–d). Microbubble phenomena of fusion (b–d, white arrows) and radiation force (d–i) can be seen, indicating that large bubbles may combine to form much larger bubbles under the influence of long vaporization pulses. Scale bars indicate 5 µm. *Note: This image comprises 9 selected frames from a longer source video. See Supplemental Data for source video.*

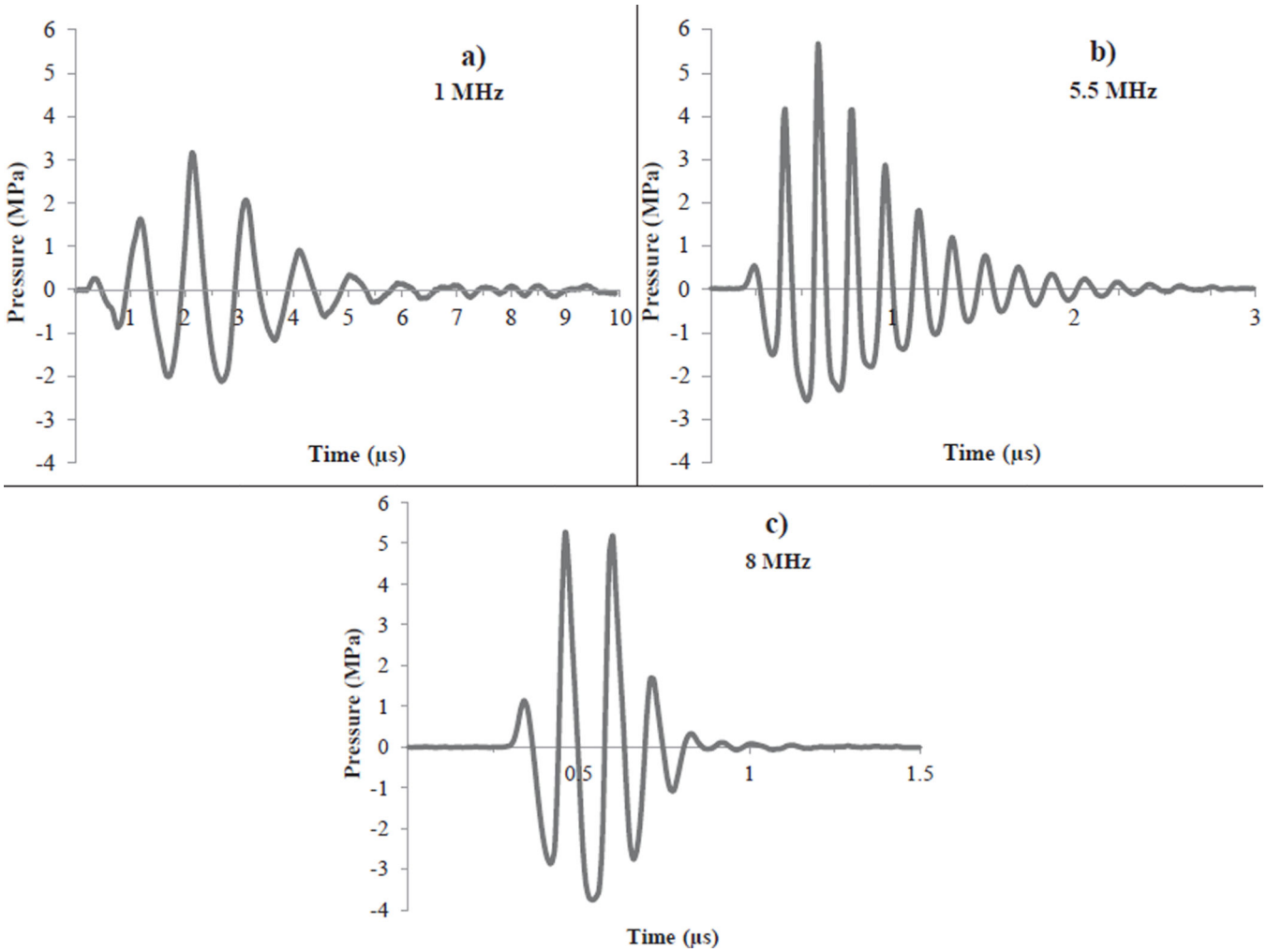

Figure 5.

Representative vaporization pulses at (a) 1, (b) 5.5, and (c) 8 MHz when driven with a 2-cycle sinusoid. Low transducer bandwidth for the high-power piston transducers resulted in additional ringing behavior such that droplets were exposed to more than just two compression/rarefaction phases. Non-linear propagation effects are clearly visible at these pressures.

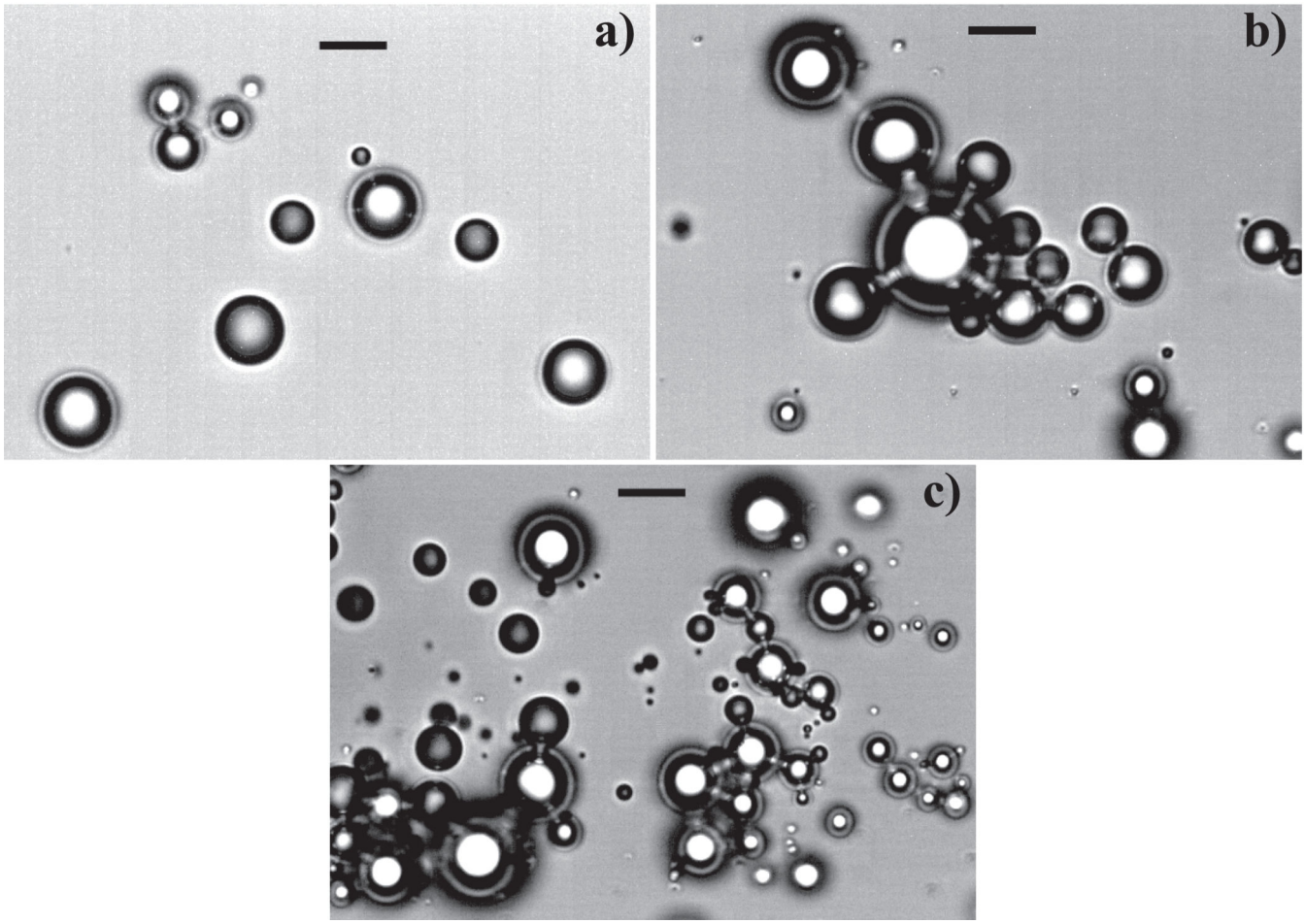

Figure 6.

Examples of bubble distributions generated as a function of ultrasound output at 5.5 MHz. At rarefactional pressures near (a) 2 MPa, few bubbles on the order of 1 μm in diameter were present, while increasing the pressure to approximately (b) 3 MPa and (c) 4.25 MPa increased the proportion of small bubbles present. Scale bar represents 5 μm.

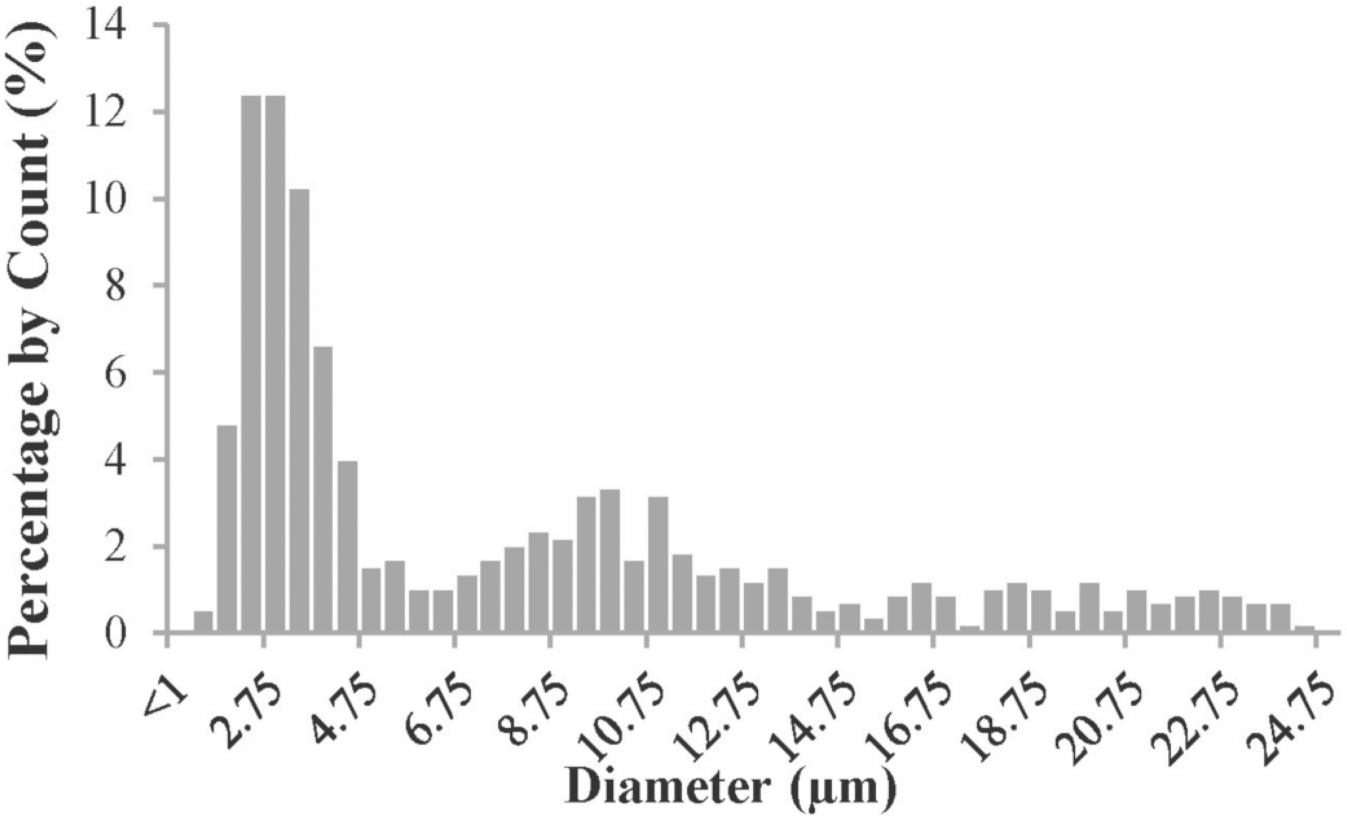

Figure 7.

Histogram of sparse bubbles present in 3 droplet emulsion samples (N=610) without the use of a vaporization pulse as a result of spontaneous thermal vaporization. Without ultrasonic vaporization, the small number of bubbles present had a mean size of 8.6 ± 3.3 μm, with a mode of approximately 3 μm.

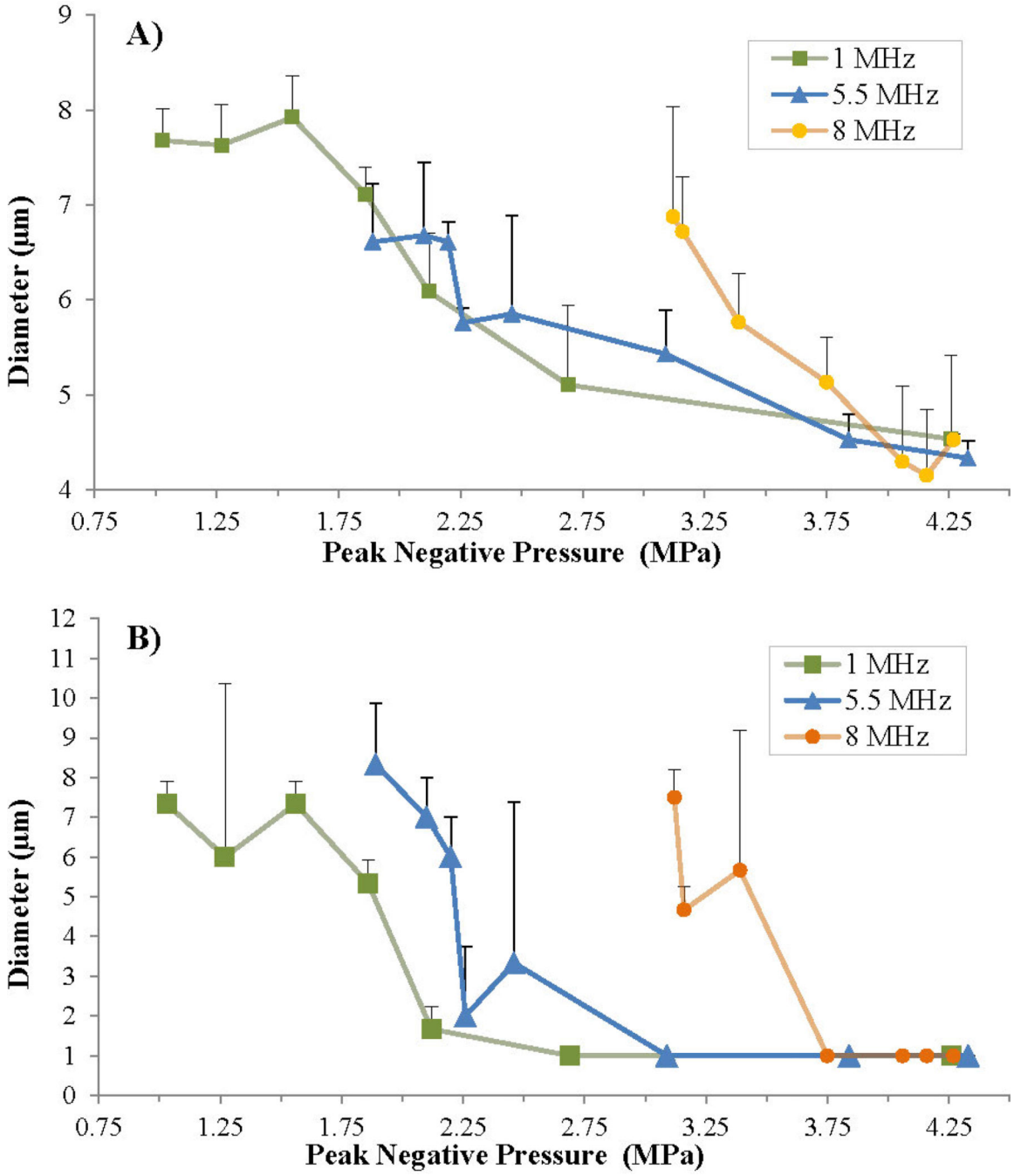

Figure 8.

Changes in distribution statistics as a function of frequency and rarefactional pressure averaged for 3 separate samples. Mean diameter (a) decreased in a generally linear fashion as rarefactional pressure increased, and all samples settled at a similar mean diameter at the highest ultrasound pressure that could be delivered. Mode diameter (b) fluctuated highly at the lowest pressures used for each frequency, but once pressures increased past a threshold, the mode settled to the lowest resolvable bin size – indicating bubbles primarily resulted

from activation of the modal peak. The rarefactional pressure required to achieve a similar mode size was seen to increase with frequency.

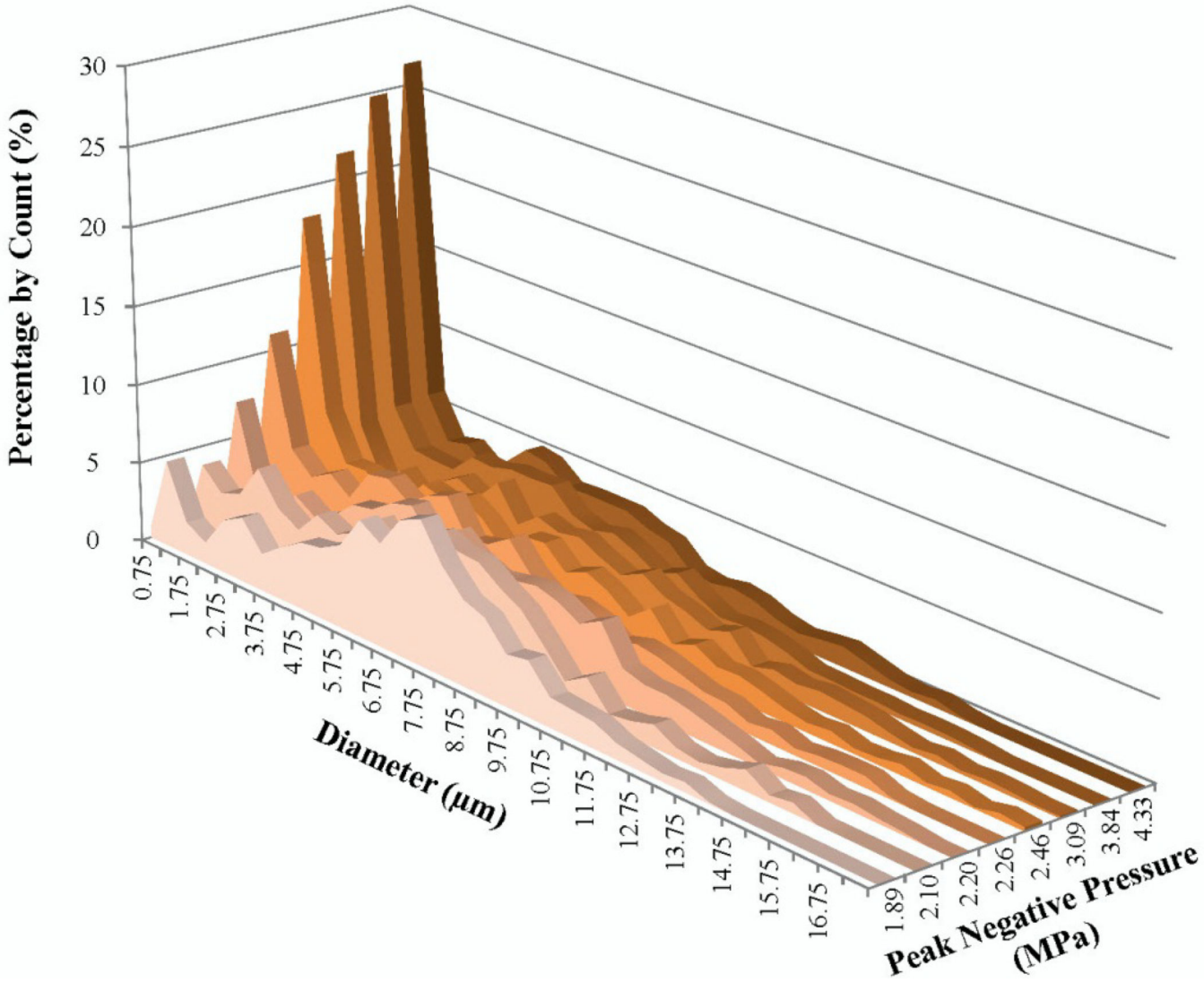

Figure 9.

Histogram of all bubble sizings taken at 5.5 MHz (N=11,654) as a function of rarefactional pressure (bin size 0.5 μm). At the lowest pressures tested, the distribution peak shifts to much higher than the controls with no ultrasound (figure 7). As pressure increases, the number of small bubbles increases in proportion until the smallest bin size overtakes as the peak in the distribution. Continued increase in the pressure amplifies the proportion of these small bubbles relative to other bubbles present in the distribution.

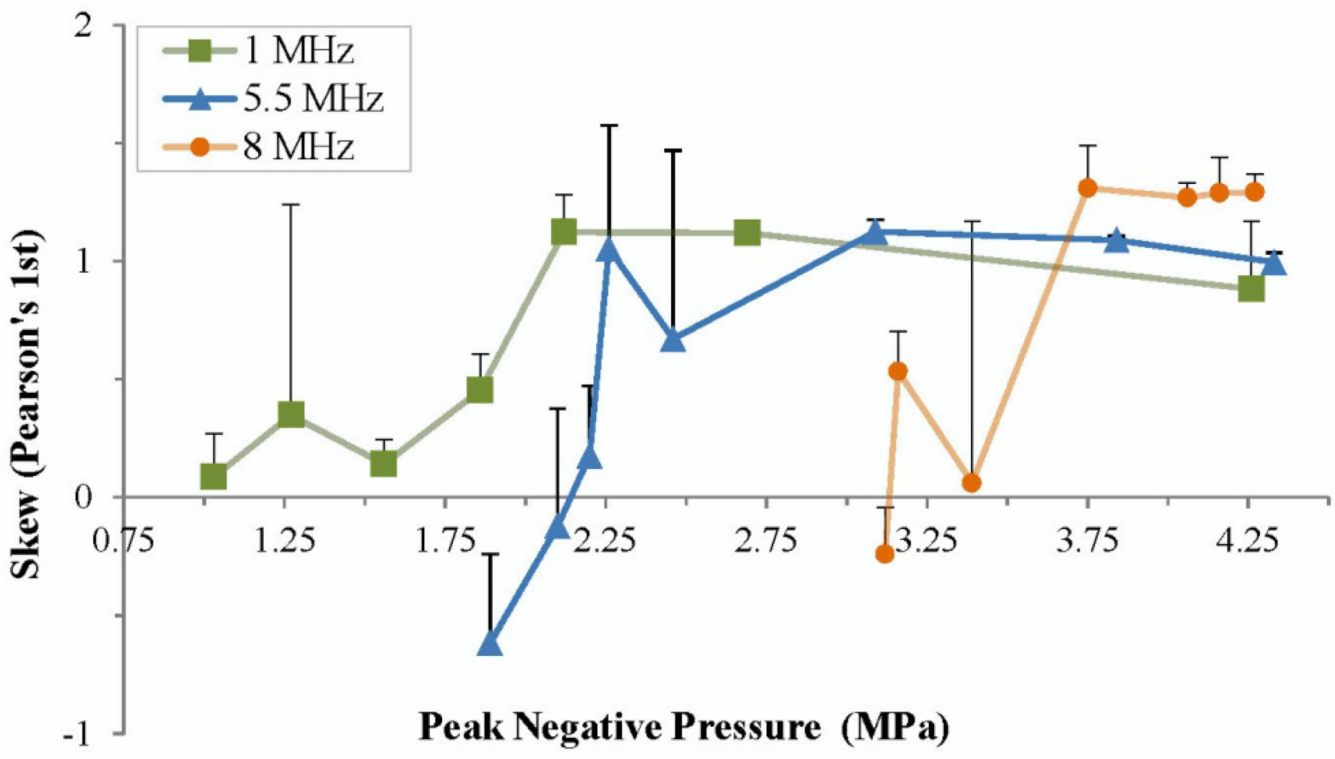

Figure 10.

Measures of distribution skew (Pearson's first skewness coefficient) averaged for all samples at each frequency. At the lowest pressures used, skew was near zero, but increased with pressure until a transitional pressure – past which skew remained constant or decreased slightly. The transitional pressure (indicating bubbles primarily resulted from nanoscale droplets in the modal peak) appears to increase with frequency.